Ultrafast Two-Photon Absorption Approach to Optical Line Shape Measurements†

L. D. Ziegler‡

Department of Chemistry, Boston University, Boston, Massachusetts 02215

Received: January 31, 2003; In Final Form: May 20, 2003

An analysis of optical heterodyne detected (OHD) two-photon absorption (TPA) resonant signals in transparent materials is presented. The formal analogies between the vibrationally resonant Raman and electronically resonant TPA $P^{(3)}$ signals and response functions are given. Fourier transform procedures are shown to allow recovery of the complex TPA response function and eliminate residual Raman contributions from these spatially selected OHD TPA responses. The phase selectivity and wavelength dependence of this technique can be exploited to reveal both the real and imaginary parts of the line shape function describing the solute−solvent response to the two-photon resonant electronic excitation. In-phase and in-quadruture measurements at any resonant wavelength yield the absorption band shape. Intramolecular vibronic structure can be determined for totally diffuse absorption bands. These effects are illustrated by the analysis of two model electronic absorption systems: the MD-simulated methyl iodide B-state origin band in Ar and a multimode Brownian-oscillator-modeled absorption line shape with simple vibronic structure. Electronic excitations less accessible to one-photon resonant ultrafast studies such as UV/VUV transition, electronic excitations in inherently optically dense media, and dipole-forbidden states are well suited for study by this TPA approach.

Introduction

A convenient framework for the organization of optical spectroscopies is given by an expansion of the induced electrical polarization in orders (n) of matter−radiation field interactions.[1−4] At any given order of this perturbative polarization description, $P^{(n)}$, the sum of all possible combinations of incident Fourier field components may result in both vibrationally and electronically resonant responses contributing to an observed spectroscopic signal, once the usual Born−Oppenheimer separation of molecular states is made. These considerations are applicable to both frequency and time domain spectroscopies, depending on the choice of detected signal frequency or signal direction, respectively. More specifically, for third-order polarization, $P^{(3)}$, ultrafast spectroscopies employing optical incident frequencies, dynamics associated with Raman-driven nuclear responses, or one-photon and two-photon electronic excitations may appear, in general, in the corresponding time-resolved signals. However, only Raman and two-photon absorption (TPA) electronic resonances can result in noninstantaneous contributions to $P^{(3)}$-derived responses when the sample is transparent (nonresonant) at the applied optical frequency.

Analogies in the treatment of vibrational Raman and two-photon electronic resonances in $P^{(3)}$ or four-wave-mixing (4WM) spectroscopies extend from the earliest conventional second-order perturbation theory[5,6,8,9] to the more recent density matrix and Hilbert space[1−4,7,10] based descriptions of molecular spectroscopy. Such a formal unified view of Raman and two-photon absorption was, in particular, highlighted by Lee and Albrecht[1] in a density matrix description of Raman and TPA, extending the direct correspondence to include resonant as well as nonresonant excitation. Experimentally, consequences of vibrational and TPA contributions at the same order of nonlinear susceptibility may be best illustrated by the cross-terms between these two amplitude-level resonances observed in CARS 4WM spectra of some transparent solutions.[2,11−13]

Time-resolved $P^{(3)}$ responses due to ultrafast-pulse-excited Raman resonances in nonresonant samples have been widely reported and well-characterized in the past decade.[4,14−19] Optical heterodyne detection, in general, linearizes the signal response and allows phase selection of the real and imaginary parts of the corresponding response function. Although the time-domain Raman technique may offer several advantages such as larger frequency and signal dynamic range, and polarization considerations, the observed nuclear responses are essentially equivalent to the Fourier transform of the conventional spontaneous Raman spectrum[4,17] and can be described as a linear free-induction decay (FID) measurement.[2] Here, we extend the formal analogy between these two $P^{(3)}$ resonances and describe the ultrafast optical-heterodyne-detected (OHD) $P^{(3)}$ responses due to electronic TPA in transparent media. The goals here are to fully characterize these novel transient OHD TPA signals, compare the consequences of vibrational versus electronic resonances on OHD responses in transparent samples, and uncover any advantages this methodology may offer for probing the properties of electronic excitations.

The OHD TPA time-domain method discussed here is distinct from the more familiar sequential resonant $P^{(3)}$ pump−probe experiments involving three resonant electronic levels, which primarily reveals population dynamics related to the one-photon resonant, intermediate electronic state.[4,20−22] In contrast, the TPA approach provides a probe of electronic coherence loss time scales. These relaxation time scales are *not* directly evident in conventional one-photon resonant pump−probe responses. The OHD TPA signal is essentially a measure of the linear electronic FID of the corresponding two-photon resonant electronic band. This technique is thus also related to the phase-locked interferometry experiments of Scherer et al. where the observed signal can be directly related to the Fourier transform of the resonant absorption band.[23−25]

† Part of the special issue "A. C. Albrecht Memorial Issue".

‡ E-mail: lziegler@chem.bu.edu.

10.1021/jp030148f CCC: $25.00
Published on Web 07/18/2003

Although no time-resolved *OHD* TPA $P^{(3)}$ responses have been reported to date, we have recently observed the homodyne response ($|P^{(3)}|^2$) due to this signal field generated by TPA resonance with the C-state of CS_2 and the B-state of CH_3I (neat liquid) at ~200 nm using ~400 nm radiation.[26,27] General expressions for the appearance of this TPA $P^{(3)}$ signal in pump−probe, homodyne, and transient grating OHD experimental configurations were derived.[26] In addition to this observation and analysis, an earlier theoretical treatment of these TPA resonances in a polarizability framework, particularly highlighting the optical-phase dependence of these signals, has been given.[28]

It should be noted at the outset that this "linear", i.e., one-time-delay, $P^{(3)}$ FID technique cannot directly distinguish the various mechanisms that may contribute to the line-broadening mechanism of a given resonant (electronic or vibrational) transition, where, for example, homogeneous and inhomogeneous broadening constitute extreme limits of spectral diffusion. In particular, optical photon echo experiments have proven successful in uncovering such solvation dynamics for strongly absorbing chromophores in solution.[29,30] However, electronic excitations less accessible to one-photon resonant ultrafast studies such as UV/VUV transitions, electronic excitations in inherently optically dense media (e.g., neat liquids and crystals), and dipole-forbidden states are especially suited for optical line shape study by this TPA approach. Finally, TPA resonances may contribute to the overall time evolution history of other spectroscopic phenomena, and thus, their characterization, with respect to transition frequencies, relative phase, and electronic coherence relaxation dynamics, may be crucial in controlling the amplitude and phase of the resulting nonlinear signals of interest. Recent examples include the two-color (400 nm/800 nm) nonlinear Raman studies of CS_2[31,32] and the three-wave, sum-frequency experiments in chiral molecular liquids[33−36] where TPA resonances provide enhancement of normally putative signals.

The potential applicability of this technique and the information that may be obtained from OHD TPA $P^{(3)}$ signals are illustrated by a detailed analysis of the simulated signals due to two TPA resonant model systems: the methyl iodide B-state origin in a rare gas solvent and a multimode Brownian oscillator (MBO) broadened electronic band with intramolecular vibronic structure. As shown below, the phase specificity of this approach allows for a measure of the real and imaginary parts of the line shape function, at least for the model cases considered here, as well as the recovery of vibrational structure from diffuse absorption bands and the determination of absorption band *shapes* from OHD TPA measurements at a single two-photon resonant excitation wavelength.

Theoretical Description

The perturbative polarization treatment of nonlinear spectroscopy is conveniently represented diagrammatically. As shown by Lee and Albrecht,[1] such a depiction readily demonstrates the analogies of the two-photon vibrationally and electronically resonant spectroscopies which appear at third order. The wave-mixing energy-level (WMEL) diagrams describing the time evolution history of two representative density matrix pathways which contribute to Raman and TPA transitions in one-photon transparent media are shown in Figure 1a. The WMEL description, formally equivalent to the double-sided Feynman diagrammatic representation, is preferred here because it conveys the relative resonant transition energy gap (electronic vs nuclear) and the nonresonant character at the applied

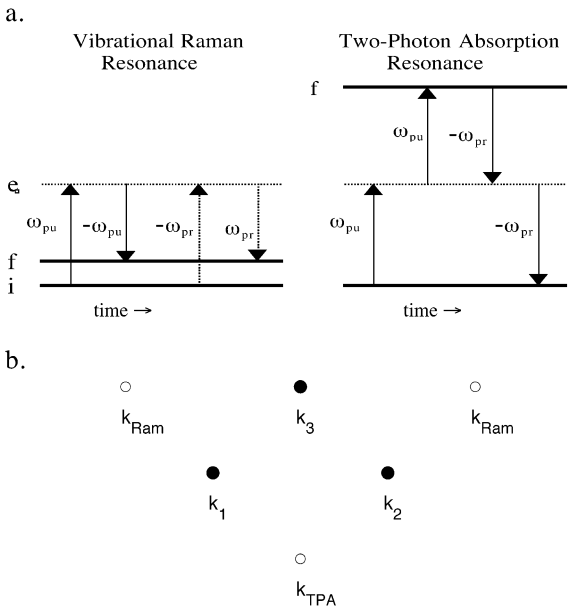

Figure 1. (a) WMEL diagrams representing density matrix time evolution histories in a three-level system contributing to vibrationally resonant, i.e., Raman, and electronically resonant, i.e., TPA, contributions to $P^{(3)}$ responses in (one-photon) nonresonant (transparent) materials. Molecular (vibronic) levels g and f correspond to the initial and resonant level; e corresponds to a virtual level. Horizontal and vertical solid/dashed lines represent real/virtual levels and bra/ket-side matter−radiation interactions, respectively. (b) A potential experimental three-incident-beam geometry for the observation of OHD TPA signals is shown. $\mathbf{k}_1$ and $\mathbf{k}_2$ correspond to the temporally overlapped pump fields from two incident beams; $\mathbf{k}_3$ and $\mathbf{k}_{TPA}$ correspond to the probe and resulting TPA signal fields ($\mathbf{k}_{TPA} = \mathbf{k}_1 + \mathbf{k}_2 - \mathbf{k}_3$). A transmissive diffractive optic results in a $\mathbf{k}_3$ probe and passively phase-locked local oscillator field along $\mathbf{k}_{TPA}$. The pu, pu, and pr Raman signal field is along the $\mathbf{k}_{Ram} = \mathbf{k}_1 - \mathbf{k}_2 + \mathbf{k}_3$ or $\mathbf{k}_2 - \mathbf{k}_1 + \mathbf{k}_3$ direction.

frequency more readily.[1,37] Virtual (nonresonant) and real vibronic state levels are represented by horizontal dotted and solid lines, respectively; bra and ket side interactions correspond to vertical dotted and solid lines, respectively.[1] The TPA resonant pathway is obtained by "folding up" vibronic level f so that it lies above intermediate level e as compared to below *e* in the Raman case.

For the $P^{(3)}$ time-domain signals of interest here, the first two field, i.e., pump, interactions are simultaneous within the pulse duration due to the material's transparency and create an electronic coherence in the TPA pathway. In contrast, a vibrational coherence is produced by the two simultaneous pump field interactions in the Raman density matrix pathway. Following the interaction of the time-delayed probe pulse, a vibrational or an electronic free-induction decay accounts for the time dependence of the OHD signal for the two density matrix histories pictured in Figure 1a. In a description limited to only rotating wave approximation (RWA) contributions for this simple three-level system, one other density matrix pathway contributes to each of these signals.[4,17,26] Electronic population decay or wave packet motion (including coherence transfer processes) on the ground or excited electronic surface characterize the analogous $P^{(3)}$ time dependence due to one-photon electronic resonance. The electronic coherence decay dynamics only affects the amplitude of the one-photon resonant pump−probe responses. These time scales, however, may be studied directly in $P^{(3)}$ photon echo based techniques when such methods are applicable.[4,29,30]

More formally, the OHD TPA resonant $P^{(3)}$ signal resulting from three identical incident fields described by **k**-

vectors ($\mathbf{k}_1$, $\mathbf{k}_2$, $\mathbf{k}_3$) with (nonresonant) carrier frequency Ω is given by[26]

$$S^{\mathrm{TPA}}_{\mathrm{OHD}}(\tau,\Delta_2,\phi) = -2\Omega\ \mathrm{Re}[e^{i\phi}(\hat{E}_{\mathrm{pr}}{}^2 \otimes \hat{E}^*_{\mathrm{pu}}{}^2 \otimes R^{\mathrm{TPA}}_{\lambda\nu\sigma\rho}(t,\Delta_2))] \quad (1)$$

$\hat{E}_{\mathrm{pu/pr}}$ represents the time envelope of the pump−probe electric field. The time-coincident ultrafast pump pulse pair ($\mathbf{k}_1$, $\mathbf{k}_2$) and the time-delayed probe ($\mathbf{k}_3$) result in a TPA signal in the $\mathbf{k}_1 + \mathbf{k}_2 - \mathbf{k}_3$ direction. In this OHD description, the local oscillator field is derived from the probe pulse and ϕ is the relative phase between the local oscillator and signal fields. The more familiar frequency-domain TPA signal (attenuation) is given by $S^{\mathrm{TPA}}_{\mathrm{OHD}}(\tau=0,\Delta_2,\phi=0)$ in the notation of eq 1. The g → f two-photon absorption response function for the three-level system defined in Figure 1 may be written as

$$R^{\mathrm{TPA}}_{\lambda\nu\sigma\rho}(t,\Delta_2) = \frac{H(t)}{\hbar} e^{2i\Omega t}\langle \hat{\alpha}_{\nu\lambda}(t)\ \hat{\alpha}_{\rho\sigma}(0)\ \hat{\rho}(-\infty)\rangle = \frac{H(t)}{\hbar}(\alpha_{\mathrm{eff,T}}{}^2)^{\mathrm{gf}} e^{-i\Delta_2 t}\, e^{-g(t)} \quad (2)$$

Δ_2 is the incident two-photon detuning from the g → f TPA transition energy, i.e., $\Delta_2 = \omega_{\mathrm{fg}} - 2\Omega$, $g(t)$ is the (complex) line shape function,[4] and $H(t)$ is the heavy-side unit step function. The polarization directions (space-fixed frame) of the two pump−probe and signal fields are ρ, σ, ν, and λ, respectively. $\hat{\alpha}$ is a polarizability operator.[28] The intensity of this signal is scaled by an effective TPA resonant polarizability, $(\alpha_{\mathrm{eff,T}}{}^2)^{\mathrm{gf}}$, defined here by

$$(\alpha_{\mathrm{eff,T}}{}^2)^{\mathrm{gf}} = \rho^{\mathrm{o}}_{\mathrm{g}}[(\alpha_{\rho\sigma})^{\mathrm{gf}} + (\alpha_{\sigma\rho})^{\mathrm{gf}}][(\alpha_{\nu\lambda})^{\mathrm{gf}} + (\alpha_{\nu\lambda})^{\mathrm{fg}}] \quad (3a)$$

where

$$(\alpha_{\rho s})^{\mathrm{gf}} = \sum_{\mathrm{e}} \frac{\mu^{\mathrm{ge}}_{\rho}\,\mu^{\mathrm{ef}}_{\sigma}}{\hbar(\omega_{\mathrm{eg}} - \Omega)} \qquad (\alpha_{\nu l})^{\mathrm{fg}} = \sum_{\mathrm{e}} \frac{\mu^{\mathrm{fe}}_{\nu}\,\mu^{\mathrm{eg}}_{\lambda}}{\hbar(\omega_{\mathrm{eg}} - \Omega)} \quad (3b)$$

$\mu^{\mathrm{ge}}_{\rho} = \langle \mathrm{g}|\hat{\mu}_{\rho}|\mathrm{e}\rangle$ is the g → e molecular electric dipole transition moment in the (space-fixed) ρth direction. The sum in the first factor of eq 3a results from the indistinguishability of the time ordering of the two nonresonant TPA pump fields; the sum in the second factor of eq 3a accounts for the two possible density matrix pathways contributing to the TPA signal field polarized along the selected λ direction. (The TPA resonance condition, $\omega_{\mathrm{fg}} = \omega_{\mathrm{fe}} + \omega_{\mathrm{eg}} = 2\Omega$, is used here to derive eq 3.) Thus, both of the density matrix pathways[26] contribute with the same sign for this TPA $P^{(3)}$ response. Integration of the TPA response function (eq 2) yields the familiar Goppert−Mayer frequency domain expression for two-photon absorption (at Δ_2) in transparent media.[1,5]

The corresponding OHD Raman response is given by[14−18]

$$S^{\mathrm{Ram}}_{\mathrm{OHD}}(\tau,\phi) = -2\Omega\ \mathrm{Re}[e^{i\phi}(I_{\mathrm{pr}} \otimes I_{\mathrm{pu}} \otimes R^{\mathrm{Ram}}_{\lambda\nu\sigma\rho})] \quad (4)$$

Within the RWA, the nonresonant Raman response function for the three-level system in Figure 1a can be similarly represented by[4]

$$R^{\mathrm{Ram}}_{\lambda\nu\sigma\rho}(t) = \frac{H(t)}{\hbar}\langle[\hat{\alpha}_{\nu\lambda}(t),\hat{\alpha}_{\rho\sigma}(0)]\rho(-\infty)\rangle = \frac{H(t)}{\hbar}(\alpha_{\mathrm{eff,R}}{}^2)^{\mathrm{gf}}\ \mathrm{Im}(e^{i\omega_{\mathrm{fg}}t}e^{-g(t)}) \quad (5a)$$

and

$$(\alpha_{\mathrm{eff,R}}{}^2)^{\mathrm{gf}} = \rho^{\mathrm{o}}_{\mathrm{g}}(\alpha_{\rho\sigma})^{\mathrm{gf}}(\alpha_{\nu\lambda})^{\mathrm{gf}} \quad (5b)$$

where we take $\omega_{\mathrm{eg}} - \Omega \approx \omega_{\mathrm{ef}} - \Omega$. In contrast to the TPA description, the classical frequency-domain Kramers−Heisenberg Raman expression is only obtained when the non-RWA terms are included in this derivation.[1] Non-RWA terms do not contribute to the TPA signal description due to the inherent electronic resonance condition, $\omega_{\mathrm{fg}} = 2\Omega$. The detuning from TPA resonance, Δ_2, plays the same role in the TPA response function defined here (eq 2) as the vibrational frequency (ω_{fg}) does in the Raman response function (eq 5a). A further distinction between these response functions is that the oscillatory character of the OHD Raman responses is independent of the off-resonant incident frequency, unlike the OHD TPA responses. In addition, the contrasting real (eq 5) vs complex (eq 2) character of the TPA and Raman OHD response functions results from the in-phase and π out-of-phase[17] contributions of the two density matrix pathways that contribute to the resonances, respectively.

Fourier transforms of the Raman response function yield the Raman spectrum once temperature effects are properly incorporated.[4,15] Analogously, the $\Delta_2 = 0$ value of the TPA response function, eq 2, is proportional to the dipole correlation function (DCF) of the g → f electronic transition here resonant at double the incident frequency. The two-photon absorption line shape ($I_{\mathrm{abs}}(\nu)$) can thus be defined in terms of the OHD TPA response function, the DCF, or the complex line shape function $g(t)$ for the three-level system (Figure 1a) by

$$I_{\mathrm{abs}}(\nu) \propto \mathrm{Re}\ \mathscr{F}\{R^{\mathrm{TPA}}(t,\Delta_2=0)\} \propto \mathrm{Re}\ \mathscr{F}\{\mathrm{DCF}(t)\} \propto \mathrm{Re}\ \mathscr{F}\{\exp(-g(t))\} \quad (6)$$

Contributions from the vibronic levels of excited state f may be included via a sum-over-all-states or equivalent approach (vide infra).

Experimental Considerations. Two experimental aspects central to the successful implementation of this TPA approach are briefly addressed here for completeness. Although OHD TPA responses have not been previously reported, strong homodyne, $|P^{(3)}|^2$, TPA signals in the $\mathbf{k}_1 + \mathbf{k}_2 - \mathbf{k}_3$ direction have been observed in some neat liquids as discussed above.[26,27] Furthermore, several schemes for detecting optical heterodyned $P^{(3)}$ Raman responses have been carried out.[18,19,38−40] However, due to the different phase-matching conditions of the TPA and Raman resonance, which allows the Raman ($\mathbf{k}_1 - \mathbf{k}_2 + \mathbf{k}_3$) and TPA electronic ($\mathbf{k}_1 + \mathbf{k}_2 - \mathbf{k}_3$) resonances to be spatially separated *beyond* the pulse overlap region (see Figure 1b), a variation of the previous "boxcar" geometries must be employed to allow heterodyne detection of this TPA $P^{(3)}$ signal field. One possible incident pulse geometry is illustrated in Figure 1b. The probe and local oscillator beams, which require relative phase stability and control, are "passively" created via a diffractive optic.[18,19,38,39] Subsequent probe field ($\mathbf{k}_3$) chopping should eliminate detection of unwanted two-beam pump−probe signals.[19] Alternatively, an active-phase stabilization scheme may be employed.[40,41]

As discussed further below, an incident pulse normalizing function at the electric field squared level, $\hat{E}_{\mathrm{pr}}{}^2 \otimes \hat{E}^*_{\mathrm{pu}}{}^2$, is required to remove incident pulse effects (finite duration and phase dispersion) from these TPA FID signals (see eq 1). One solution is incident pulse characterization via FROG or some equivalent methodology.[42,43] Additionally, a material with a large *nonresonant* electronic response that masks any nuclear con-

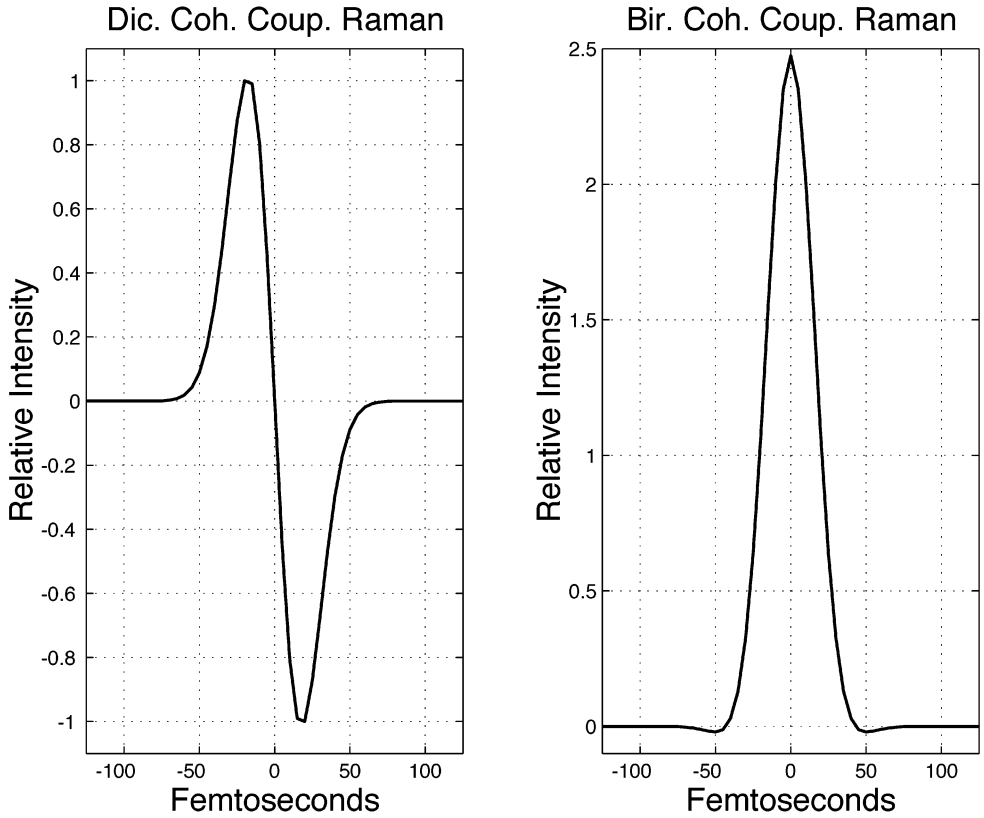

Figure 2. Modeled coherent coupling (pu, pr, pu) dichroic and birefringent responses due to the Raman response of methanol for linearly chirped, 35 fs Gaussian pulses.

tributions can be used to generate the required field squared correlation function. Polarization considerations may be exploited to eliminate the Raman contributions in the TPA direction for such a procedure.[44]

Elimination of Pulse-Overlapping Raman Contributions. Due to the direction of the detected OHD TPA $P^{(3)}$ signal, $\mathbf{k}_1 + \mathbf{k}_2 - \mathbf{k}_3$, where $\mathbf{k}_1$ and $\mathbf{k}_2$ (pump) pulses are always temporally coincident, Raman responses due to the field time orderings $\mathbf{k}_1 - \mathbf{k}_3 + \mathbf{k}_2$ and $\mathbf{k}_2 - \mathbf{k}_3 + \mathbf{k}_1$ (pu, pr, pu) can only contribute to the detected signal for transparent samples when all three incident fields overlap in time. These nuclear contributions in the sequential TPA direction are due to impulsive Raman excitation from a temporally overlapped pump field ($\mathbf{k}_1$ or $\mathbf{k}_2$) and a probe field ($\mathbf{k}_3$), and are given by[26]

$$S_{\mathrm{OHD}}^{\mathrm{Ram}}(\tau) = -2\Omega\ \mathrm{Re}\ e^{i\phi}\int_{-\infty}^{+\infty} dt\ \hat{E}_{\mathrm{pr}}(t-\tau)\ \hat{E}_{\mathrm{pu}}^{*}(t) \times \int_{0}^{\infty} d\tau'\ \hat{E}_{\mathrm{pr}}^{*}(t-\tau-\tau')\ \hat{E}_{\mathrm{pu}}(t-\tau')\ R^{\mathrm{Ram}}(\tau') \quad (7)$$

The responses due to this coherence coupling term are either symmetric (even) or antisymmetric (odd) with respect to the interpulse delay (τ) for birefringent ($\phi = \pi/2$) or dichroic ($\phi = 0$) OHD measurements, respectively, when the Raman response function is predominantly real. Calculated phase-specific coherence coupling responses due to the anisotropic Raman response of methanol[16] excited by linearly chirped (1.2 times the transform-limited bandwidth) 35 fs Gaussian pulses are shown in Figure 2 and demonstrate this symmetry effect. Consequently, by taking the real (imaginary) part of the Fourier transform of the dichroic (birefringent) observed signal, the effects of these Raman contributions can be selectively eliminated from the responses detected in the TPA direction ($\mathbf{k}_1 + \mathbf{k}_2 - \mathbf{k}_3$). Thus, the real and imaginary parts of the TPA response function, convoluted with the pulse characteristics, may be obtained when both $\phi = 0$ and $\phi = \pi/2$ measurements are made. Such a Fourier transform procedure is employed to separate nonresonant electronic responses from Raman responses in OHD ultrafast Raman spectroscopy (OKE).[15] Furthermore, since these coherence coupling terms depend on pulse temporal overlap, the relative contribution of these terms will decrease as the pulse duration is decreased. Judicious polarization configurations may also be utilized to discriminate against unwanted nuclear-driven contributions.[44]

Vibronic Considerations: Allowed vs Forbidden TPA Transitions, TPA vs Raman. The relative cross-sections of the vibrationally resonant (Raman) and electronically resonant (TPA) $P^{(3)}$ contributions will be, in part, dependent on the symmetry characteristics of the electronic state reached by the TPA. No nuclear coordinate dependence of the molecular transition polarizability needs to be considered for a two-photon allowed electronic excitation aside from Franck−Condon effects. In contrast, the Raman polarizability *requires* the nuclear coordinate dependence of the molecular transition polarizability for this vibrational transition to emerge once the usual Born−Oppenheimer separation of molecular states is made. Thus, if we expand the molecular transition polarizability in powers of nuclear coordinates (Q_a) around the ground-state equilibrium configuration in the usual fashion

$$\alpha \approx \alpha_o + (1/2)\sum_a (\partial\alpha/\partial Q)_o Q_a + \ldots \quad (8)$$

the typical ratio of leading terms, α_o:$\alpha' Q$, is 10:1.[45] Thus, the TPA resonant cross-section should be about 100 times larger than a Raman transition (finite temperature effects aside) and, hence, readily observable in solutions. Vibronic coupling involving the appropriate nontotally symmetric nuclear coordinates can also bring allowed character to one-photon or

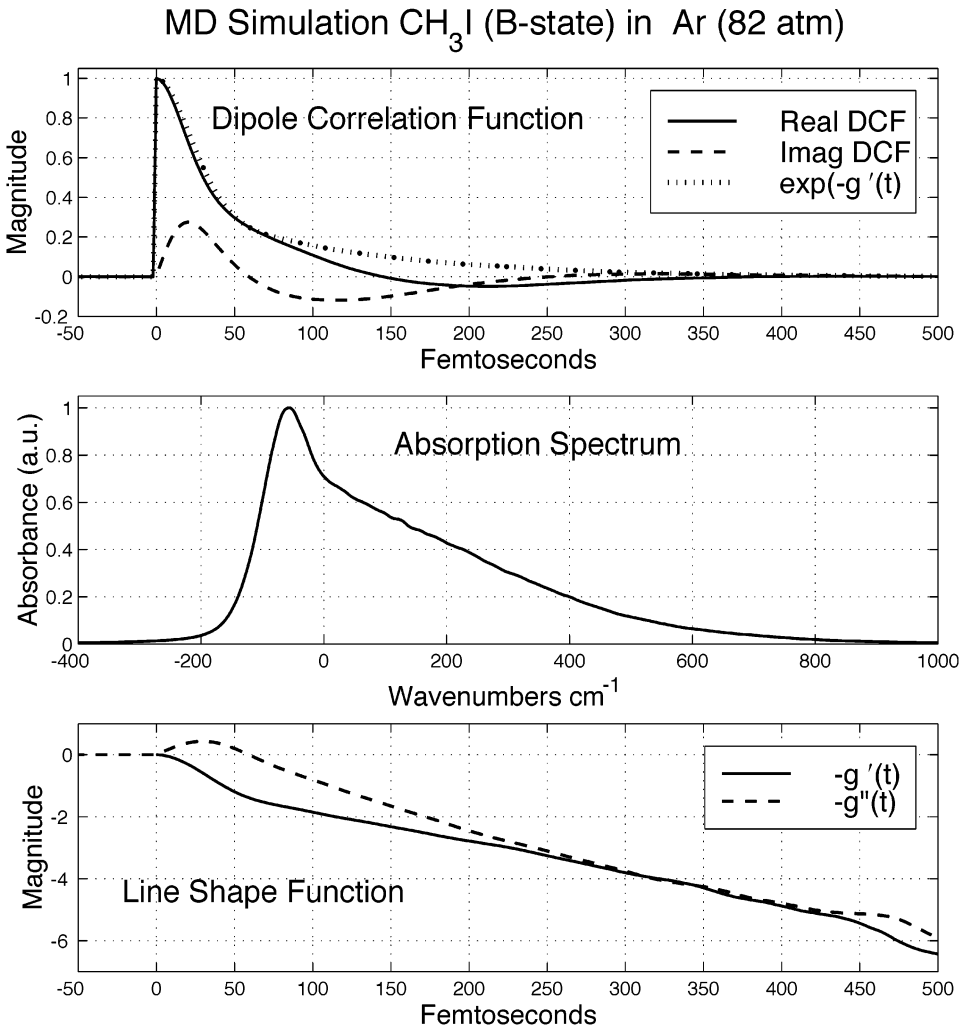

Figure 3. MD-simulated dipole correlation function corresponding to the methyl iodide B-state origin band in 82 atm of Ar. The corresponding absorption band shape, and real ($g'(t)$) and imaginary ($g''(t)$) line shape components resulting from this simulation are also given.

two-photon forbidden transitions as is well-known. Thus, for such dipole-forbidden TPA resonances the corresponding TPA time-domain response may be on the same order as a typical Raman response and thus should be at least observable in neat solutions and moderately concentrated solutions. This vibronic TPA mechanism is analogous to the well-known B-term of Raman scattering activity[46] and the vibronic mechanism responsible for the appearance of resonance hyper-Raman scattering from centrosymmetric molecules.[47] In terms of the vibronic TPA response function, the only formal effect of the promoting vibronic transition moment is to introduce a factor of $\exp(-i\omega_a t)$ in eq 2, which simply shifts the electronic resonance to the "false origin", as has been previously noted.[28]

OHD TPA Signal Simulations and Analysis

The first step in making use of experimental OHD TPA responses to obtain a time-domain description of the TPA resonant absorption band is to eliminate the effects of the pulse temporal characteristics from these observables and recover the complex TPA response function. This can be accomplished by a Fourier transform procedure that is analogous to that routinely used for the recovery of the Raman impulse response function from femtosecond OHD (OKE) birefringence measurements in one-photon *and* two-photon transparent materials.[15] As evident from eq 1, the phase-specific response function can be determined from experimentally observed OHD TPA responses by the following deconvolution scheme:

$$\text{Re } R^{\text{TPA}}(t,\Delta_2) = \mathcal{F}\{\text{Re } R^{\text{TPA}}(\omega,\Delta_2,\phi{=}0)\}\, H(t) \quad (9a)$$

$$\text{Im } R^{\text{TPA}}(t,\Delta_2) = \mathcal{F}\{-[\text{Im } R^{\text{TPA}}(\omega,\Delta_2,\phi{=}\pi/2)]\}\, H(t) \quad (9b)$$

where

$$R^{\text{TPA}}(\omega,\Delta_2,\phi) = \frac{\mathcal{F}\{S^{\text{TPA}}_{\text{OHD}}(\tau,\Delta_2,\phi)\}}{\mathcal{F}\{{E_{\text{pr}}}^2 \otimes {E^*_{\text{pu}}}^2\}} \quad (9c)$$

As eqs 9a−c reveal, once an accurate $\hat{E}_{\text{pr}}{}^2 \otimes \hat{E}^{*\,2}_{\text{pu}}$ autocorrelation is determined at a given detuning (Δ_2), the complex TPA impulse response function can be recovered from $\phi = 0$ and $\phi = \pi/2$ measurements at that incident frequency. This normalization accounts for both finite pulse duration and phase distortion (e.g., chirp) effects. By selecting the real and imaginary parts of the TPA response function spectral densities, $R^{\text{TPA}}(\omega,\Delta_2,\phi)$, the symmetry characteristics of the temporally and remaining spatially overlapping Raman contributions (Figure 2) are exploited to eliminate these unwanted signals in the TPA direction as discussed above.

The value and potential applicability of this TPA technique are illustrated below by modeling OHD TPA measurements in

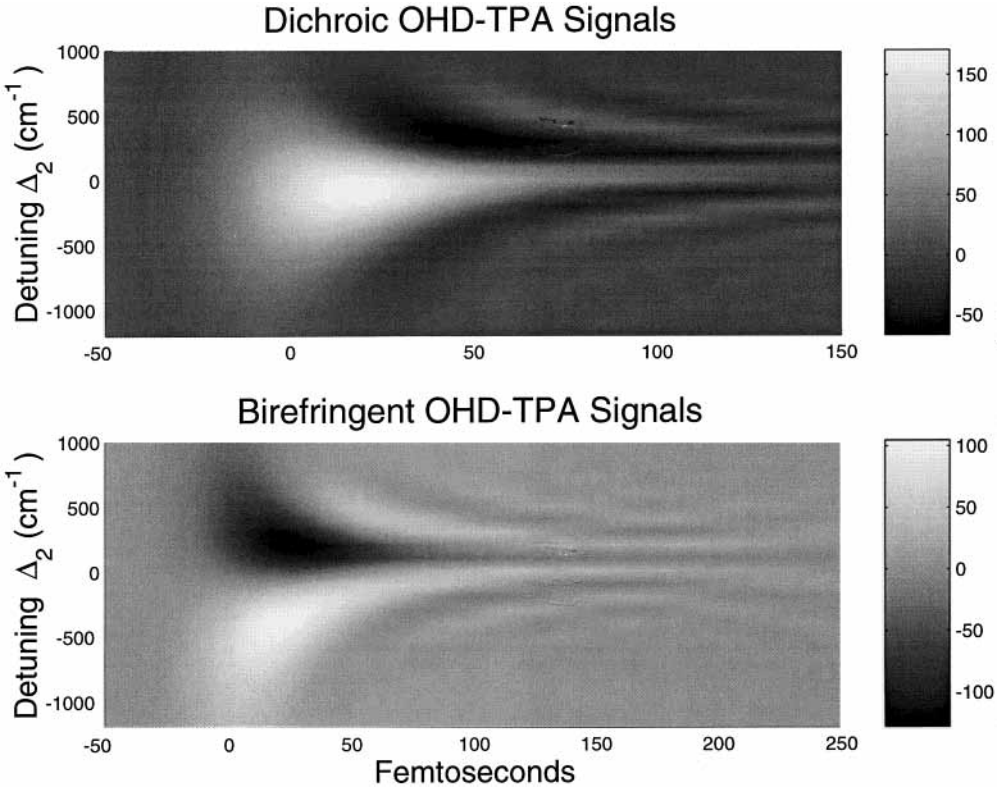

Figure 4. Dichroic ($\phi = 0$) and birefringent ($\phi = \pi/2$) OHD TPA signals due to linearly chirped (1.2 times the transform-limited bandwidth) 35 fs pulses as a function of detuning from the two-photon resonance, Δ_2, for the simulated CH_3I in Ar system.

two relatively simple solute−solvent absorption systems. In part, these two absorptions are chosen because the models of solute−solvent line broadening are different in these systems and correspond to two widely used approaches for incorporating short-time solvent effects in optical line shape analyses.

B-State of CH_3I. On the basis of the observed density-dependent absorption and resonance emission characteristics of the B-state origin band of methyl iodide in some nonpolar gases, we have determined the corresponding solute−solvent pair potentials.[48−50] This very strong one- and two-photon allowed absorption feature is located at ∼201 nm and is widely separated (∼1100 cm^{-1}) from the accompanying weaker Franck−Condon structure. MD simulations employing these "experimental" potentials determined the DCF and energy correlation function corresponding to this electronic origin in high pressures of Ar and CH_4.[49,50] The experimentally derived potentials were subsequently used to study solvation effects in these solutions.[51−53] Agreement between theory and experiment was judged largely on the basis of the similarity between the density-dependent observed absorption line shapes and the Fourier-transformed MD-calculated DCFs, and the subsequent agreement between observed and calculated Raman/resonance fluorescence excitation profiles. The MD-generated DCFs which have been experimentally verified in this fashion are used here to illustrate the nature of the predicted OHD TPA signals due to resonance with this UV transition.

Optical line shape studies of this chromophore are of interest as an electronic excitation probe of short-time solvation dynamics across a large range of available densities/pressures, including the supercritical fluid region and its corresponding interpretation in terms of SCF solvating behavior and theoretical treatments of solvation effects such as INM and mode-coupling theory.[51,52,54] Photon echo studies (e.g., 3PEPS) resonant with this excitation are probably not viable due to the required near-VUV ultrafast pulse wavelengths and complications (vide infra) from solvent TPA effects.[55] Thus, the efficacy of this TPA approach, using blue radiation for probing the details of this far-UV optical line shape, is examined here.

The real and imaginary parts of the MD-simulated DCF corresponding to the CH_3I B-state origin in 82 atm of Ar ($\rho^* = 0.08$)[49−51] are displayed in Figure 3 (upper panel). Details about these simulations may be found elsewhere.[49] This ensemble decay is dominated by inhomogeneous effects at this bath density. Multiple time scales are clearly evident in these DCF decays due to the (non-Gaussian) distribution of initial transition energies. Consequently, a multimode Brownian oscillator model truncated at second order in a cummulent expansion, commonly used to describe solvation in room-temperature solutions,[4,29,30] is not applicable here. The corresponding absorption spectrum, given by the real part of the Fourier-transformed DCF is also shown in Figure 3. Zero wavenumbers on the abscissa corresponds to the gas-phase (solvent → ∞) electronic transition frequency in this model.[49] This origin band line shape is identical for both the one- and two-photon resonances as defined here (see eq 6).

If the DCF is represented in terms of a complex line shape function,[4,29,30] $g(t) = g'(t) + ig''(t)$, then the imaginary part of the DCF ($\sin(g''(t)\exp(-g'(t))$ relates to the fluorescence Stokes shift or solvent reorganizational energy (at least within linear response constraints). A predicted Stokes shift of ∼110 cm^{-1} is evident from the simulation results in Figure 3 (middle panel). As illustrated here, the decays due to the real and imaginary parts of the line shape function (Figure 3, lower panel) are distinct from those of the DCF for this absorption band. For example, the decay due to the real part of the line shape function, $\exp(-g'(t))$, in contrast to that due to the real part of the DCF, monotonically decreases for this system (Figure 3, upper panel). Without more information than just the absorption band shape, it is difficult to determine the precise unsolvated transition frequency particularly when the transition frequency distribution

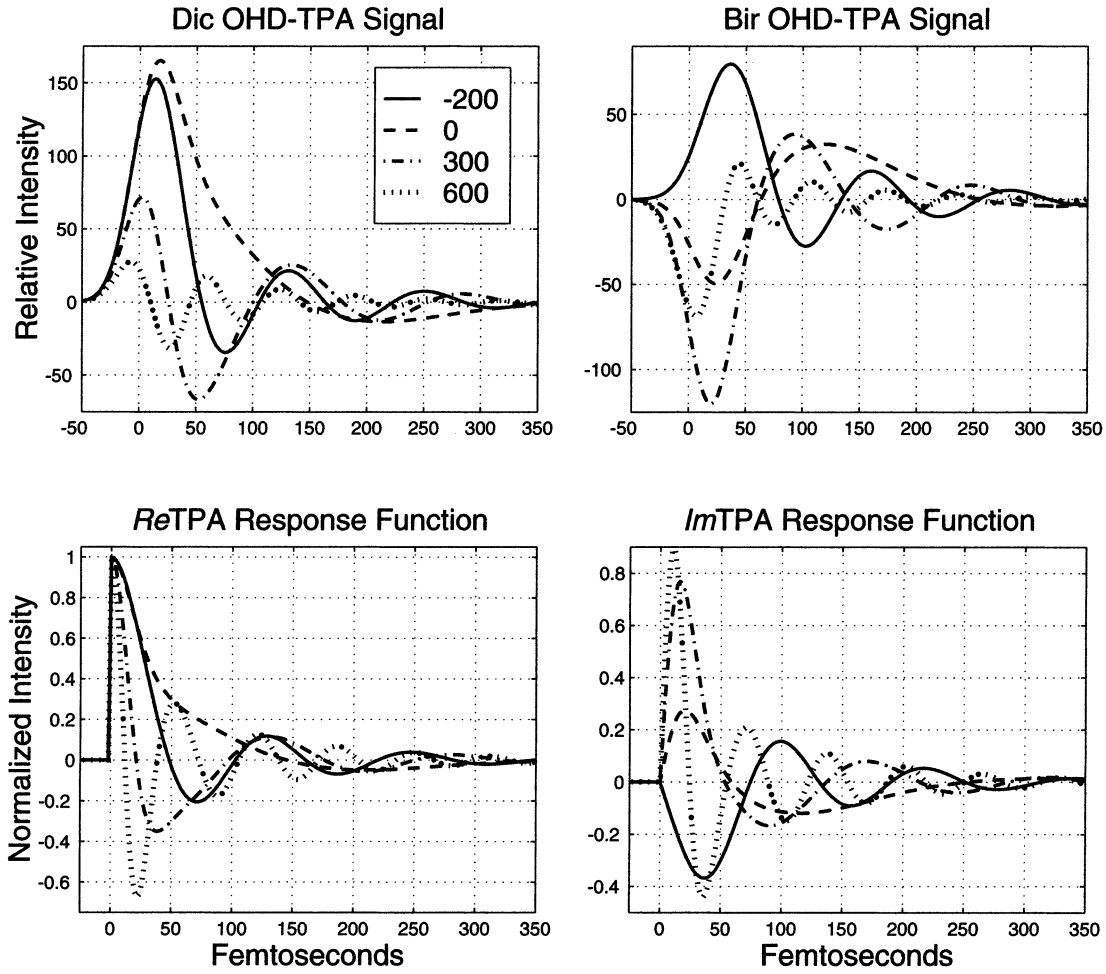

Figure 5. Simulated dichroic ($\phi = 0$) and birefringent ($\phi = \pi/2$) OHD TPA signals and the corresponding real and imaginary parts of the TPA response function at the indicated detunings (cm^{-1}) for the simulated CH_3I in Ar system.

is not governed by a central limit theorem result. Hence, Fourier transforms of the simulated DCFs were used to compare experimental and MD simulation results in the previous simulation studies.[49]

The in-phase and in-quadruture OHD responses due to TPA with this simulated absorption line shape excited by linearly chirped 35 fs Gaussian pulses (1.2 times the transform-limited bandwidth) as a function of the incident carrier frequency from the (gas-phase) 0−0 transition frequency are represented by a 2D plot in Figure 4. Linearly chirped pulses are employed in this simulation to more realistically simulate experimental conditions and demonstrate that the analysis of line shape character is not compromised by the phase distortions characterizing laboratory pulses. The nearly even- and oddlike symmetry characters with respect to Δ_2 of the dichroic and birefringent OHD TPA responses, respectively, are evident in these surfaces for this isolated electronic origin band absorption. Representative phase-specific TPA responses, corresponding to slices through the Figure 4 surfaces, for four detunings are displayed in Figure 5 (upper panels). By employing the Fourier transform procedure described above (eqs 9a−c), the TPA response functions, at these selected detunings, given in the lower panels of Figure 5, can be experimentally determined. Thus, once the appropriate field autocorrelation function is found, the relaxation character at the earliest times, generally attributable to inertial effects, can be exposed by this direct time-domain procedure. The oscillations evident in these responses (Figure 5) arise from the detuning (Δ_2) dependence of the TPA response function and the imaginary character of the line shape function ($g''(t)$).

The decay due to the real part of the line shape function can be obtained from the TPA response functions recovered by the procedure described above when dichroic and birefringent OHD TPA measurements are both made at any detuning wavelength. More specifically, for the TPA response function given by eq 2 for a single resonant absorption feature at any incident near-resonant two-photon wavelength

$$e^{-g'(t)} \propto [\mathrm{Re}\, R^{\mathrm{TPA}}(t,\Delta_2)^2 + \mathrm{Im}\, R_{\mathrm{TPA}}(t,\Delta_2)^2]^{1/2} \qquad (10)$$

Thus, the phase specificity of this OHD TPA methodology in principle allows $g'(t)$ to be determined unambiguously, at least for relatively isolated resonances.

Furthermore, once the complex TPA response function is specified by deconvolution of the $\phi = 0$ and $\pi/2$ OHD TPA measurements, the two-photon resonant absorption band *shape* can also be recovered. Given the form of $R^{\mathrm{TPA}}(t,\Delta_2)$ defined in eq 2, the Fourier transform (real part) of this function yields the absorption band shape displaced by Δ_2 from the true 0−0 frequency:

$$I_{\mathrm{abs}}(\nu+\Delta_2) \propto \mathrm{Re}\, \mathscr{F}\{R^{\mathrm{TPA}}(t,\Delta_2)\} \qquad (11)$$

Consequently, at each TPA resonant frequency the absorption band shape can, in principle, be recovered for this single absorption feature system when both in-phase and in-quadruture TPA responses are observed.

Additional information regarding the "true" origin (0−0) of the band shape is required, however, to determine the imaginary

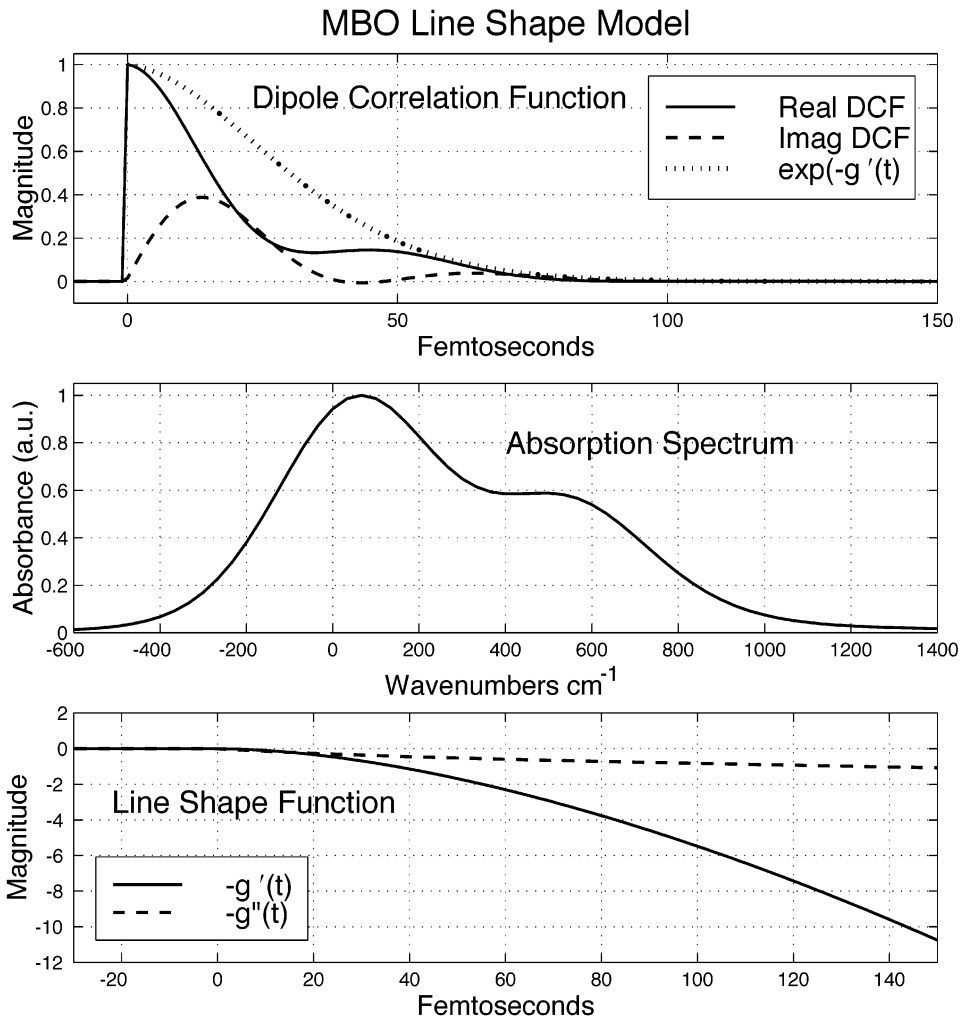

Figure 6. Dipole correlation function corresponding to a modeled absorption system consisting of an origin band and one vibronic mode (500 cm^{-1}). Spectral broadening due to solute−solvent coupling is given by an MBO model (see the text for model details). The corresponding absorption band shape and real ($g'(t)$) and imaginary ($g''(t)$) line shape components for this model system are also given.

part of the line shape function ($g''(t)$) for the simulated band shape of interest here. We note that the absorption intensity at a given detuning is found by integrating the TPA response function (eq 2) over the delay time. Thus, wavelength-dependent TPA responses also determine the absolute energy of the TPA. For the $\Delta_2 = 0$ detuning incident frequency the Fourier-transformed response function (eq 11) will be coincident with that of the absolute TPA line shape. Once the incident frequency corresponding to $\Delta_2 = 0$ is found, then $g''(t)$ is directly given by a tan((Im $R^{TPA}(t,\Delta_2=0)$)/(Re $R^{TPA}(t,\Delta_2=0)$)).

Solute−Solvent Coupling via a Brownian Oscillator Model. In the second illustration of OHD TPA analysis two-photon resonance with an absorption band with vibronic structure and solute−solvent coupling described by an MBO model of solvation dynamics is considered. This MBO description is widely used in the analysis of nonlinear ultrafast spectroscopies and optical line shape studies for condensed-phase systems where electronic coherence loss dynamics are often characterized by multiple time scales.[4,29,30] In this model, the complex line shape function, $g(t)$, is determined once the normalized transition energy correlation function, $M(t)$, is specified:

$$g(t) = i\lambda \int_0^t dt'\, M(t') + \langle \Delta\omega^2 \rangle \int_0^t dt' \int_0^{t'} dt''\, M(t'') \quad (12)$$

The solvent (intermolecular) reorganization energy, λ, is related, in the high-temperature limit, to the (Gaussian) static transition energy distribution or coupling strength, $\langle \Delta\omega^2 \rangle^{1/2}$, by $\langle \Delta\omega^2 \rangle = 2k_B T\lambda/\eta$, resulting in a solvent Stoke shift of 2λ.[4,29,30]

Here we take the relaxation of $M(t)$ to result from two representative[29] components: $M(t) = 0.65 \exp(-t^2/70^2) + 0.35 \exp(-t/1000)$ in units of femtoseconds. Furthermore, in contrast to the methyl iodide simulation above, nuclear *intra*molecular coupling will be modeled by a 500 cm^{-1} vibronic component damped by the same solvent relaxation mechanism as the origin band, with half the absorption strength. Thus, the OHD TPA response function for this system is given by

$$R^{TPA}(t,\Delta_2) = e^{-i\theta(t)}(e^{-g'(t)} + a e^{i\omega_v t} e^{-g'(t)}) \quad (13)$$

where $\theta(t) = \Delta_2 t + g''(t)$, $a = 0.5$, and $\omega_v = 500$ cm^{-1}. The real and imaginary parts of the dipole correlation function ($R^{TPA}(t,\Delta_2 = 0)$) and the line shape function and the resulting absorption band shape are shown in Figure 6 for the absorption band described by the MBO model defined above. This model absorption system exhibits diffuse vibronic structure (middle panel in Figure 6). As evident from the absorption spectrum, the Stokes shift (2λ) for this absorption system is ~140 cm^{-1}. As compared to the CH_3I in Ar model (Figure 3), the decays of the real part of the DCF and the line shape function are faster (sub-100 fs) and $g''(t)$ decays monotonically for the MBO model system.

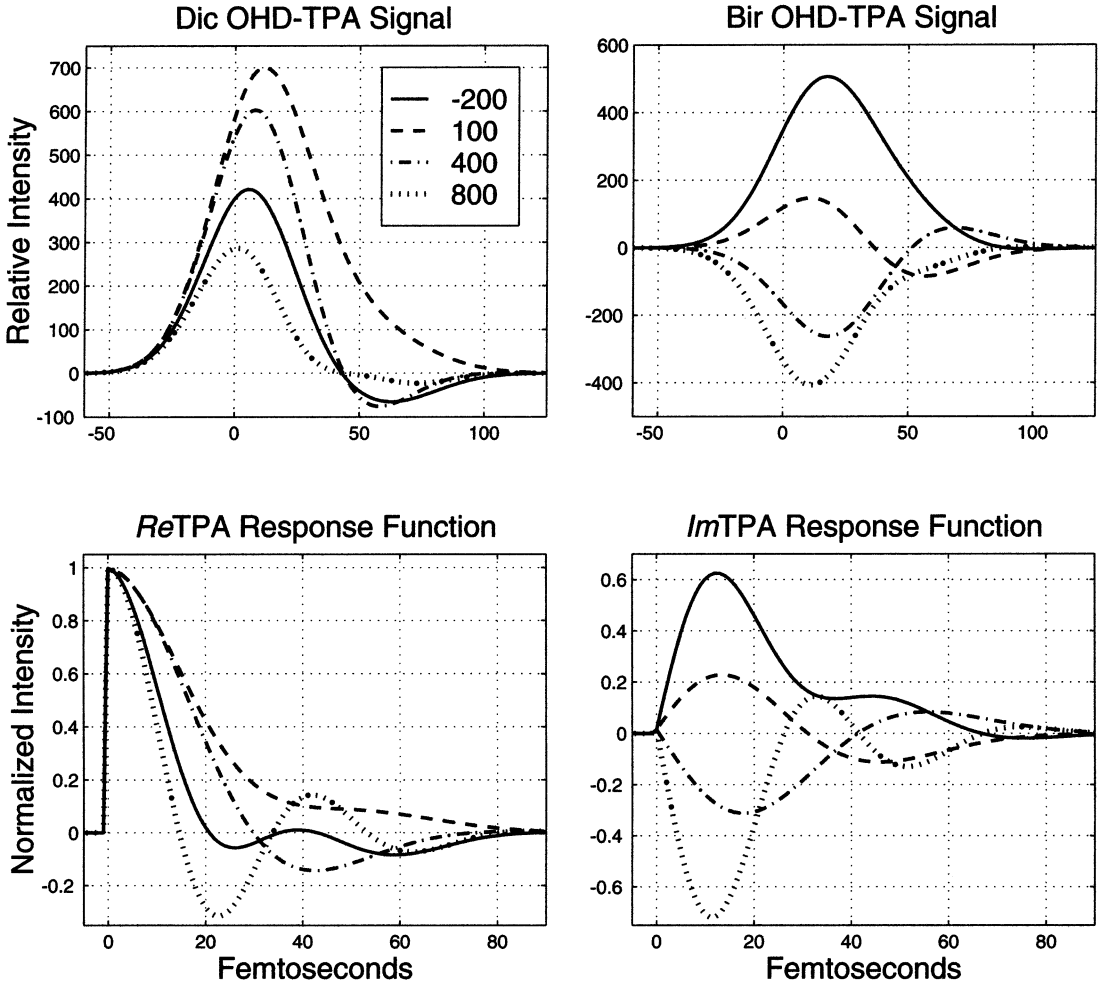

Figure 7. Simulated dichroic ($\phi = 0$) and birefringent ($\phi = \pi/2$) OHD TPA signals and the corresponding real and imaginary parts of the TPA response function at the indicated detunings (cm^{-1}) for the modeled MBO vibronic system.

The birefringent and dichroic OHD TPA simulated signals at four incident wavelengths two-photon resonant with this absorption band excited by linearly chirped, 35 fs Gaussian pulses are shown in Figure 7. Following pulse deconvolution (eqs 9a−c), the real and imaginary parts of the OHD TPA response function (eq 13) are derived from these simulated signals at each of these detunings and are also displayed in Figure 7.

The question addressed here is what can be learned about the nature of the TPA resonant electronic transition from the complex $R^{TPA}(t,\Delta_2)$, which is the product of these OHD ultrafast experiments, as compared to, for example, cw TPA attenuation measurements yielding the absorption band shape alone. A time-dependent phase factor, $\psi(t,\Delta_2) = a\tan((\mathrm{Re}\ R^{TPA}(t,\Delta_2))/(\mathrm{Im}\ R^{TPA}(t,\Delta_2)))$ can be constructed from the complex TPA response function at each resonant frequency, Δ_2. Oscillatory components due to the detuning (Δ_2), the line shape function ($g''(t)$), and vibronic structure (ω_v) contribute to this $\psi(t,\Delta_2)$. Fourier transforms of $\psi(t,\Delta_2)$ for the model MBO absorption system, $\psi(\nu,\Delta_2)$, at four incident wavelengths clearly show (see Figure 8) the intramolecular mode contribution at 500 cm^{-1} (and its overtone). The sign-flipping low-frequency feature peaking at $\sim$35 cm^{-1} is exclusively due to the resonant detuning (Δ_2) and $g''(t)$.

Although an *estimate* of the ω_v vibrational frequency can also be determined from some TPA attenuation or action spectrum for the model absorption band (Figure 6), issues of precision aside, the ability of this time-domain technique to uncover underlying vibronic structure is greater than that simply due to absorption band shape fitting. A modeled diffuse absorption band system consisting of two vibronic bands at 400 and 600 cm^{-1} with relative coupling strengths of 2:1, respectively, and MBO line shape description is shown in Figure 9 (left-hand panel). No vibronic features are discernible in this model absorption band. The corresponding $\psi(\nu,\Delta_2)$ derived from in-phase and in-quadruture TPA OHD measurements at $\Delta_2 = 50$ cm^{-1}, however, clearly exhibits the two vibronic bands and their 2:1 relative coupling ratio (Figure 9). Oppositely phased combination and overtone frequency components are also evident. Thus, underlying vibrational structure may be resolved from analysis of the OHD TPA response functions even when the corresponding two-photon resonant absorption band is vibrationally diffuse.

The vibronic structure complicates the retrieval of the real part of $g(t)$ as compared to the isolated CH_3I absorption band discussed above. However, fitting procedures based on the phase-specific TPA responses may be developed to extract the line shape function, at least for relatively simple vibronically structured bands. As an example, we consider the electronic absorption band corresponding to the TPA response function defined by eq 13 (Figure 6). The real part of the line shape function ($g'(t)$) can be readily shown to be given by

$$e^{-g'(t)} = \left[\frac{(\mathrm{Re}\ R^{TPA}(t,\Delta_2))^2 + (\mathrm{Im}\ R^{TPA}(t,\Delta_2))^2}{1 + a^2 + 2a\cos(\omega_v t)}\right]^{1/2} \quad (14)$$

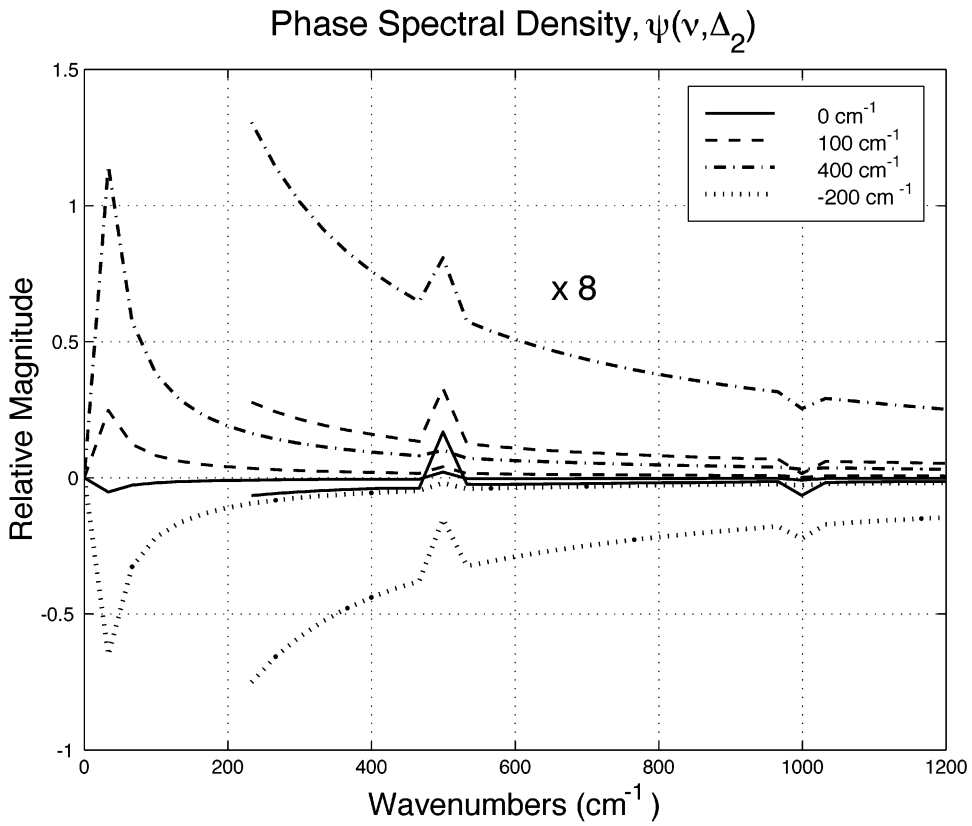

Figure 8. Fourier transform of the TPA response function phase, $\psi(\nu,\Delta_2)$, as a function of incident frequency detuning from TPA for the model absorption spectrum shown in Figure 6. The 500 cm^{-1} vibronic component is clearly evident at all incident TPA wavelengths.

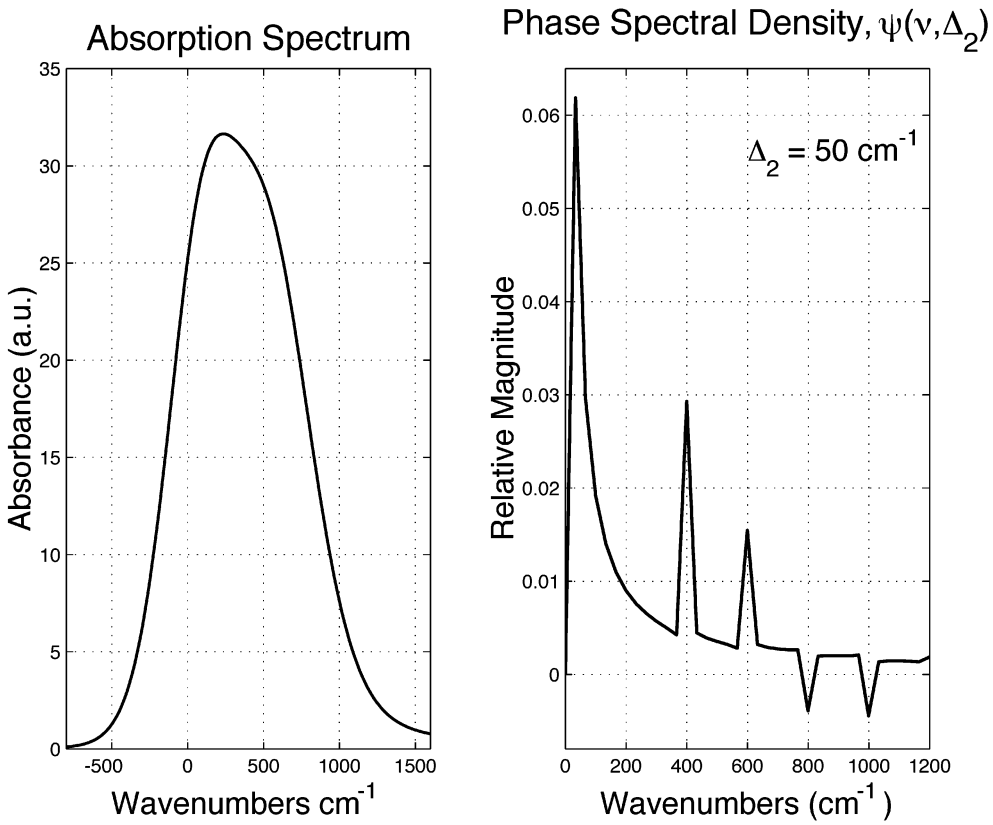

Figure 9. Fourier transform of the TPA response function phase, $\psi(\nu,\Delta_2)$, at $\Delta_2 = 50$ cm^{-1} is given in the right side panel for the diffuse MBO model absorption spectrum pictured in the left panel. This absorption band shape results from an origin band and vibronic features at 400 and 600 cm^{-1} broadened by an MBO description for the solvent coupling. The 400 and 600 cm^{-1} vibronic components are clearly evident in $\psi(\nu,\Delta_2)$ although entirely obscured in the absorption band.

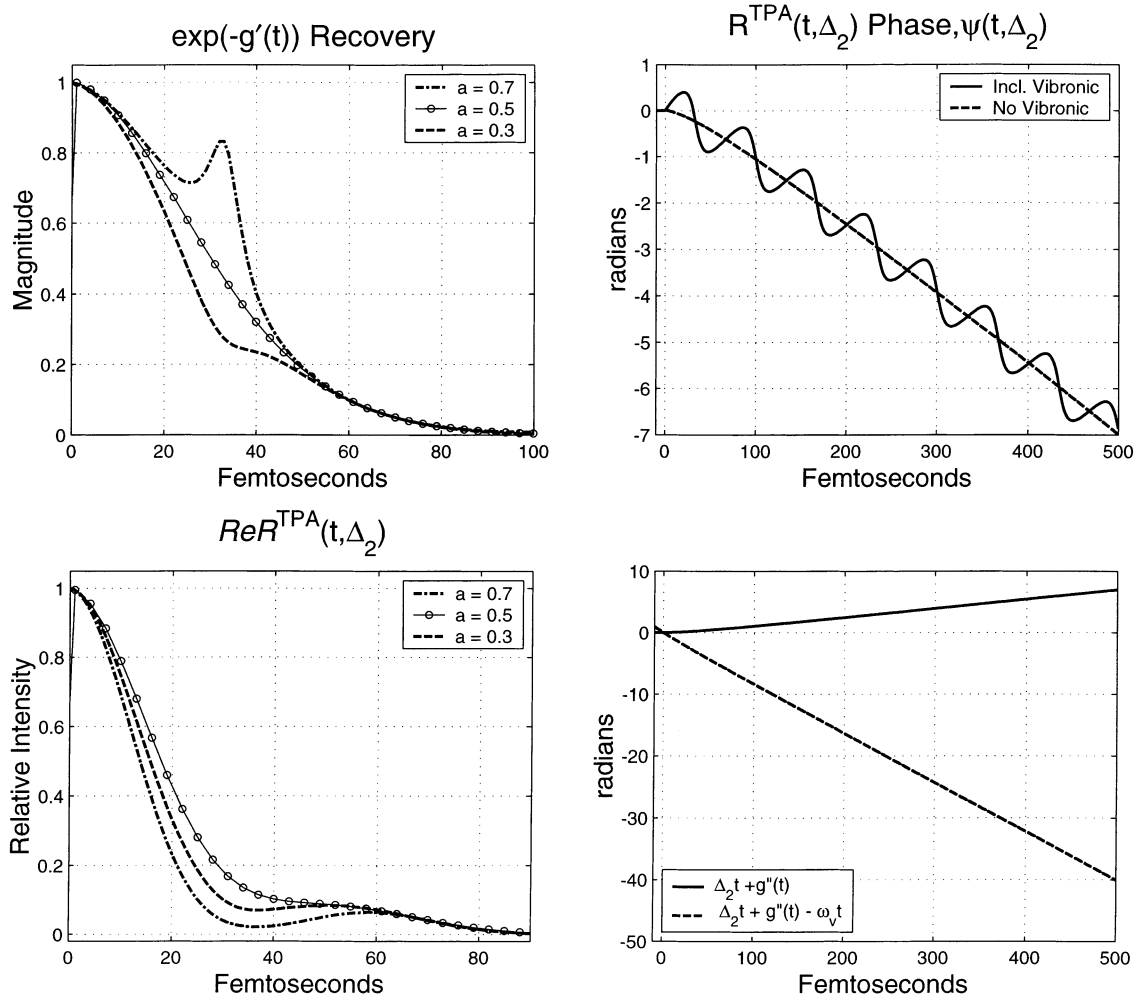

Figure 10. A procedure is demonstrated for the recovery of the real part, $g'(t)$ of the MBO contribution to the line shape derived from the real and imaginary parts of the TPA response function for the absorption system pictured in Figure 6. a is the magnitude of the coupling strength for the 500 cm^{-1} vibronic component. (See the text for more details.)

Re $R^{TPA}(t,\Delta_2)$ and Im $R^{TPA}(t,\Delta_2)$ are the experimentally determined quantities, and $\psi(\nu,\Delta_2)$, the Fourier transform of the phase factor $\psi(t,\Delta_2) = a \tan((\text{Re } R^{TPA}(t,\Delta_2))/(\text{Im } R^{TPA}(t,\Delta_2)))$, reveals ω_v as described previously and demonstrated in Figure 8. Thus, the coupling strength, a, is the only additional parameter needed to find $g'(t)$ via eq 14. When $\omega_v = 0$, $\psi(t,\Delta_2) = \theta(t,\Delta_2)$ for this model system as eq 13 indicates. Hence, by filtering, i.e., by removing, the underdamped $\omega_v = 500$ cm^{-1} vibronic component from $\psi(\nu,\Delta_2)$, and then inverse Fourier transforming the remaining $\psi(\nu,\Delta_2)$ spectral density, an experimentally based measure of $\theta(t,\Delta_2)$ is obtained. The results of this filtering procedure are shown in Figure 10 (upper and lower right panels) for an excitation frequency of $\Delta_2 = 100$ cm^{-1}. When this vibronic filtered phase, $\theta(t,\Delta_2)$, is substituted in eq 13, a best fit of the "experimental" Re $R^{TPA}(t,\Delta_2)$ and that due to eq 13 determines the required coupling strength parameter, a, as shown in Figure 10 (lower left panel). The experimental Re $R^{TPA}(t,\Delta_2)$ response is indicated by circles in this figure. The corresponding $g'(t)$ values (eq 14) are given in the upper left panel of Figure 10.

When $\exp(-g'(t))$ can be determined over a large dynamic range with good signal/noise ratio, the corresponding $M(t)$ and $g''(t)$ can in principle be found for the MBO solvation model (via eq 12). A more sophisticated, optimized fitting procedure than that described here based on the phase-specific TPA responses at multiple resonant wavelengths is needed to determine $g'(t)$ for absorption systems with larger numbers of vibronically active modes.

Finally, as discussed above for the CH_3I MD line shape example, the real part of the Fourier transform of the determined OHD TPA response functions (eq 13) for this MBO-broadened vibronic absorption system yields the resonant TPA band shape shifted by Δ_2 from its true band position. However, the absolute band shape is found by integration of these response functions. Hence, as in the previous section, the $\Delta_2 = 0$ frequency can in principle be determined by this methodology. As discussed above, at $\Delta_2 = 0$ the real part of the Fourier transform of the complex TPA response function is coincident with the TPA band spectrum. The responses at $\Delta_2 = 0$ can then be used to find the imaginary part of the line shape function, $g''(t)$, since the other parameters, $g'(t)$, ω_v, and a, are already determined for this model absorption system.

Conclusions

The original premise for this study was to extend the earlier treatment of vibrational (Raman) and electronic (TPA) $P^{(3)}$ resonances for frequency domain spectroscopy, which highlighted the equivalence of these molecular transitions,[1] to OHD ultrafast time-domain measurements. However, owing to the controllable phase selectivity and wavelength dependence of the corresponding $P^{(3)}$ OHD responses, the OHD electronic TPA approach appears likely to be a more useful probe of resonant

line shape character than its Raman analogue. This additionally reflects the more significant inter- and intramolecular coupling resulting from electronic excitation as compared to the nuclear coupling due to vibrational resonance. Analysis of the OHD TPA signals for the model absorption systems considered here reveals the real and imaginary parts of the line shape function, which describes the bath coupled response to the electronic excitation, and the vibrational structure and relative coupling strengths due to the intramolecular coupled nuclear degrees of freedom, even for vibrationally diffuse absorption spectra. Thus, the information available from these OHD TPA linear FID measurements is well in excess of that obtained by simply measuring the Fourier transform of the resonant absorption spectrum.

Aside from providing these specific determinations of the resonant optical line shape characteristics, the direct time-domain FID measurements generally offer better experimental tests of theory. Often, for example, the dipole correlation function is the primary calculated quantity in classical and mixed quantum-classical molecular dynamics based simulations of absorption features. The usually greater dynamic range of the time-domain measurements as compared to that derived from absorption spectra provides a basis for much more detailed comparisons with computational results. This is especially important for descriptions of short-time dynamics which requires information often buried in the wings of optical spectra. The larger signal dynamic range is particularly useful when multiple time scales (or mechanisms) contribute to the total electronic dephasing process. Furthermore, Fourier transforming the optical line shape to report a DCF is problematic for most solute−solvent systems, due to the inherent uncertainty in the true electronic origin resulting from solvation, intramolecular coupling, and dynamical processes on the resonant excited-state surface, as well as problems due to baseline determinations.

The OHD TPA methodology explored here is at least another potential tool for the spectroscopic study of optical transition line shapes. Again, we underscore that this one-dimensional method has no capability to directly temporally resolve different relaxation mechanisms contributing to the optical line shape as might result from an optical photon echo (PE) based measurement. However, determinations of the real and imaginary parts of the line shape function ($g(t)$) over a relatively large dynamics range of times can potentially afford a measure of the underlying energy correlation function within a multimode Brownian oscillator model. The functional form of this fitted $M(t)$ may be interpreted in terms of the dynamical components of the corresponding solvation processes.

As mentioned above, this TPA methodology is particularly suited for the study of electronic excitations less accessible to one-photon resonant (PE) ultrafast measurements. Examples include (1) learning about electronic coherence loss dynamics of UV/VUV transitions beyond the one-photon resonant reach of current short pulses which can thus be probed with just visible or near-UV pulses by this technique, (2) studies of dephasing dynamics of inherently optically thick materials, such as neat liquids or crystals, because the TPA signal is obtained with one-photon *nonresonant* incident radiation, and (3) absorption studies (transition frequency and optical dephasing dynamics) of one-photon forbidden but TPA allowed electronic states such as the lowest lying singlet states of polyenes. The next step in the development of this additional ultrafast probe of electronic line shapes is clearly the experimental observation of these OHD TPA signals. Such efforts are currently under way in our laboratory.

References and Notes

(1) Lee, D.; Albrecht, A. C. In *Advances in Infrared and Raman Spectroscopies*; Clark, R. J. H., Hester, R. E., Eds.; Wiley: Heyden, 1985; Vol. 12, p 179.

(2) Levenson, M. D.; Kano, S. S. *Nonlinear Laser Spectroscopy*; Academic Press: New York, 1988.

(3) Boyd, R. W. *Nonlinear Optics*; Academic Press: San Diego, 1992.

(4) Mukamel, S. *Nonlinear Optical Spectroscopy*; Oxford University Press: Oxford, 1995.

(5) Goppert-Mayer, M. *Ann. Phys. (Leipzig)* **1931**, *9*, 273.

(6) Plazcek, G. *Rayleigh and Raman Scattering*; UCRL Trans. No. 5262 from *Handbuk der Radiologie*; Marx, E., Ed.; Leipzig Akademische Verlagsgesellschaft: Leipzig, Germany, 1934; Vol. VI, Chapter 2, pp 209−374.

(7) Bloembergen, N. *Nonlinear Optics*; W. A. Benjamin: Reading, MA, 1977.

(8) Peticolas, W. L. *Annu. Rev. Phys. Chem.* **1967**, 18.

(9) McClain W. M.; Harris, R. A. In *Excited States*; Lim, E. C., Ed.; Academic Press: New York, 1977; Vol. 3, pp 1−56.

(10) Loudon, R. *The Quantum Theory of Light*; Oxford University Press: Oxford, 1973.

(11) Lotem, H.; Lynch, R. T., Jr.; Bloembergen, N. *Phys. Rev. A* **1976**, *14*, 1748.

(12) Liao, P. F.; Bjorklund, G. C. *Phys. Rev. Lett.* **1976**, *36*, 584.

(13) Lynch, R. T., Jr.; Lotem, H. *J. Chem. Phys.* **1977**, *66*, 1905.

(14) McMorrow, D.; Lotshaw, W. T.; Kenney-Wallace, G. A. *IEEE J. Quantum Electron.* **1988**, *24*, 443.

(15) McMorrow D.; Lotshaw, W. T. *Chem. Phys. Lett.* **1990**, *174*, 85.

(16) Cho, M.; Du, M.; Scherer, N. F.; Fleming G. R.; Mukamel, S. *J. Chem. Phys.* **1993**, *99*, 2410.

(17) Ziegler, L. D.; Fan, R.; Desrosiers, A. E.; Scherer, N. F. *J. Chem. Phys.* **1994**, *100*, 1823.

(18) Khalil, M.; Demirdoven, N.; Golonzka, O.; Fecko, C. J.; Tokmakoff, A. *J. Phys. Chem. A* **2000**, *104*, 5711.

(19) Xu, Q.-H.; Ma Y.-Z.; Fleming, G. R. *Chem. Phys. Lett.* **2001**, *338*, 254.

(20) Materny, A.; Lienau. C.; Zewail, A. H. *J. Phys. Chem.* **1966**, *100*, 18650.

(21) Dantus, M.; Rosker, M. J.; Zewail, A. H. *J. Chem. Phys.* **1987**, *87*, 2395; **1988**, *89*, 6128.

(22) Scherer, N. F.; Jonas, D. M.; Fleming, G. R. *J. Chem. Phys.* **1993**, *99*, 153.

(23) Scherer, N. F.; Carlson, R. J.; Matro, A.; Du, M.; Ruggerio, A. J.; Romero-Rochin, V.; Cina, J. A.; Fleming G. R.; Rice, S. A. *J. Chem. Phys.* **1991**, *95*, 1487.

(24) Scherer, N. F.; Matro, A.; Ziegler, L. D.; Du, M.; Carlson, R. J.; Cina, J. A.; Fleming, G. R. *J. Chem. Phys.* **1992**, *96*, 4180.

(25) Ziegler, L. D.; Scherer, N. F. *J. Chem. Phys.* **1992**, *97*, 4704.

(26) Ziegler, L. D.; Jordanides, X. J. *Chem. Phys. Lett.* **2002**, *352*, 270.

(27) Jordanides, X. J.; Ziegler, L. D. Unpublished results.

(28) Kawashima, H.; Nelson, K. A. *J. Chem. Phys.* **1994**, *100*, 6160.

(29) Joo, T.; Jia, Y.; Yu, J.-Y.; Lang, M. J.; Fleming, G. R. *J. Chem. Phys.* **1996**, *104*, 6089.

(30) Fleming, G. R.; Cho, M. *Annu. Rev. Phys. Chem.* **1996**, *47*, 109.

(31) Astinov, V.; Kubarycha, K. J.; Milne, C. J.; Miller, R. J. D. *Chem. Phys. Lett.* **2000**, *327*, 334.

(32) Kubarych, K. J.; Milne, C. J.; Lin, S.; Astinov V.; Miller, R. J. D. *J. Chem. Phys.* **2002**, *116*, 2016.

(33) Belkin, M. A.; Kulakov, T. A.; Ernst, K.-H.; Yan, L.; Shen, Y. R. *Phys. Rev. Lett.* **2000**, *85*, 4474.

(34) Belkin, M. A.; Han, S. H.; Wei, X.; Shen, Y. R. *Phys. Rev. Lett.* **2001**, *87*, 113001.

(35) Fischer, P.; Beckwitt, K.; Wise, F. W.; Albrecht, A. C. *Chem. Phys. Lett.* **2002**, *352*, 463.

(36) Fischer, P.; Albrecht, A. C. *Bull. Chem. Soc. Jpn.* **2002**, *75*, 1119.

(37) Ulness, D. J.; Kirkwood, J. C.; Albrecht, A. C. *J. Chem. Phys.* **1998**, *108*, 3897.

(38) Maznev, A. A.; Nelson, K. A.; Rogers, J. A. *Opt. Lett.* **1998**, *23*, 1319.

(39) Goodno, G.; Dadusc, G.; Miller, R. J. D. *J. Opt. Soc. Am. B* **1998**, *15*, 1791.

(40) Matsuo, S.; Tahara, T. *Chem. Phys. Lett*. **1997**, *264*, 636.

(41) Kaufman, L. J.; Heo, J.; Ziegler, L. D.; Fleming, G. R. *Phys. Rev. Lett.* **2002**, *88*, 207402.

(42) Kane, D. J.; Trebino, R. *IEEE J. Quantum Electron.* **1993**, *29*, 571.

(43) Iaconis, C.; Walmsley, I. A. *IEEE J. Quantum Electron.* **1999**, *35*, 501.

(44) Etchepare, J.; Grillon, G.; Chambaret, J. P.; Hamoniaux, G.; Orszag, A. *Opt. Commun*. **1987**, *63*, 329. Tokmakoff, A. *J. Chem. Phys*. **1996**, *105*, 1.

(45) Ziegler, L. D.; Albrecht, A. C. *J. Chem. Phys.* **1974**, *60*, 3558. Albrecht, A. C. Electronic Spectroscopy Gordon Conference presentation, La Jolla, CA, 2001.
(46) Tang, J.; Albrecht, A. C. In *Raman Spectroscopy*; Szymanski, H. A., Ed.; Plenum Press: New York, 1970; Vol. 2. Albrecht, A. C.; Hutley, M. C. *J. Chem. Phys.* **1971**, *55*, 4438.
(47) Chung, Y. C.; Ziegler, L. D. *J. Chem. Phys.* **1988**, *88*, 7287.
(48) Halpern, A. M.; Ziegler, L. D. *Chem. Phys. Lett.* **1989**, *161*, 1.
(49) Kalbfleisch, T.; Fan, R.; Roebber, J.; Moore, P.; Jacobsen E.; Ziegler, L. D. *J. Chem. Phys.* **1995**, *103*, 7673.
(50) Fan, R.; Kalbfleisch, T.; Ziegler, L. D. *J. Chem. Phys.* **1996**, *104*, 3886.
(51) Kalbfleisch, T. S.; Ziegler, L. D.; Keyes, T. *J. Chem. Phys.* **1996**, *105*, 7034.
(52) Kalbfleisch, T. S.; Ziegler, L. D. *J. Chem. Phys.* **1997**, *107*, 9878.
(53) Everitt, K. F.; Geva, E.; Skinner, J. L. *J. Chem. Phys.* **2001**, *114*, 1326.
(54) Bagchi B.; Bhattacharyya, S. *Adv. Chem. Phys.* **2001**, *116*, 67.
(55) Zimdars, D.; Francis, R. S.; Ferrante C.; Fayer, M. D. *J. Chem. Phys.* **1997**, *106*, 7498.